1 **Nonlinear responses of particulate nitrate to NOₓ emission controls in**

2 **the megalopolises of China**

3   Mengmeng Li[1, *], Zihan Zhang[1], Tijian Wang[1], Min Xie[1], Shu Li[1], Bingliang Zhuang[1]

4   and Yong Han[2]

5 [1] School of Atmospheric Sciences, Nanjing University, Nanjing 210023, China

6 [2] Guangdong Province Key Laboratory for Climate Change and Natural Disaster

7 Studies, School of Atmospheric Sciences, Sun Yat-Sen University, Guangzhou, China

8 [*] Corresponding author: mengmengli2015@nju.edu.cn

9 **Abstract**

10   Nitrate is an increasingly important component of fine particulate matter ($PM_{2.5}$)

11 in Chinese cities. The production of nitrate is not only related to the abundance of its

12 precursor, but also supported by atmospheric photochemical oxidants. The control of

13 nitrogen oxides (NO_x) emissions may thereby lead to nonlinear changes of nitrate

14 concentrations, raising a new challenge to the current emission control actions in

15 China. This paper uses comprehensive measurements and a regional meteorology-

16 chemistry model with optimized mechanisms to establish the nonlinear responses

17 between particulate nitrate and NO_x emission controls in the megalopolises of China.

18 Nitrate is an essential component of $PM_{2.5}$ in eastern China, accounting for 9.4–15.5%

19 and 11.5–32.1% of the $PM_{2.5}$ mass for the warm and cold seasons. The hypothetical

20 NO_x emission reduction scenarios (−10%~−80%) during summer-autumn result in

21 almost linearly lower $PM_{2.5}$ by −2.65% in Beijing-Tianjin-Hebei (BTH) and −2.79%

22 in Yangtze River Delta (YRD) per 10% cut of NO_x emissions, whereas they increase

23 the oxidant levels and lead to a rather complicated response of PM components in

24 winter. Wintertime nitrate is found to increase by 4.28% in BTH and 4.60% in YRD,

25 with higher dinitrogen pentoxide (N_2O_5) intermediate products produced from

26   increased ozone introduced by lower NO_x emissions. An inflexion point appears at

27   40–50% NO_x emission reduction, and a further cut in NO_x emission is predicted to

28   cause −8.74% reduction of nitrate for BTH and −10.59% for YRD per 10% cut of

29   NO_x emissions. In addition, the 2012–2016 NO_x control strategy actually leads to no

30   change or even increase of nitrate in some areas (8.82% in BTH and 14.41% in YRD)

31   during winter. This paper helps understand the nonlinear aerosol and photochemistry

32   feedbacks, and defines the effectiveness of proposed mitigations for the increasingly

33   serious nitrate pollution in China.

1 Introduction

36   Secondary inorganic aerosols (SIA), including sulfate (SO_4^{2-}), nitrate (NO_3^-) and

37   ammonium (NH_4^+) account for 30–60% of the total fine particulate matter ($PM_{2.5}$)

38   mass during haze events in China (Huang et al., 2014a; Zhao et al., 2013). Since the

39   enactment of the Air Pollution Action Plan in 2013, the Chinese government has

40   taken drastic measures to reduce the emissions of sulfur dioxide (SO_2), nitrogen

41   oxides (NO_x) and primary $PM_{2.5}$, leading to significant decreases in sulfate and

42   overall $PM_{2.5}$ concentrations in cities (Silver et al., 2018; Li et al., 2021a; Wang et al.,

43   2017). Meanwhile, the nitrogen/sulfur (N/S) ratio in $PM_{2.5}$ increased significantly and

44   nitrate had been the main component of $PM_{2.5}$ (16–45%) during haze episodes,

45   despite a more than 20% reduction in the concentrations of its precursor NO_x (Shao et

46   al., 2018; Wen et al., 2018; Zhai et al., 2019). The increasingly serious nitrate

47   pollution has emerged to be the new emphasis of air pollution controls in China.

48   Nitrate formation involves complex multiphase chemical reactions. In the

49   daytime, nitrogen dioxide (NO_2) reacts with hydroxyl radical (OH) to produce nitric

50   acid (HNO_3). With excess ammonium (NH_3), low temperature and insufficient

51   sulphuric acid, this reaction can proceed quickly and produce high ammonium nitrate

52   (Seinfeld and Pandis, 2006). In the nighttime, however, high-concentration NO_2 reacts

53   with ozone (O_3) to produce the nitrate radical (NO_3) and dinitrogen pentoxide (N_2O_5).

54   The heterogeneous hydrolysis of N_2O_5 on wet particles is the main pathway for

55   nocturnal nitrate formation (56–97%) (He et al., 2018; Pathak et al., 2011; Xue et al.,

56   2014).

57   Nitrate chemistry is not only related to the abundance of its precursor NO_x, but

58   also supported by atmospheric oxidants (OH and O_3) produced from the

59   photochemical reactions of NO_x and volatile organic compounds (VOC_s) (Meng et al.,

60 1997). Using a box model, some studies have determined that the relationship

61 between particulate nitrate and NO_x emissions is nonlinear depending on the ozone

62 chemical sensitivity regime (Pun and Seigneur, 2001; Nguyen and Dabdub, 2002).

63 Pun and Seigneur (2001) showed that the daytime HNO_3 production was more

64 sensitive to the concentration of atmospheric oxidants, and that in the VOC-limited

65 regime the decrease of HNO_3 production due to the NO_x emission control might be

66 offset by the increase of OH. Nguyen and Dabdub (2002) calculated a detailed

67 isopleth between nitrate and NO_x emission; they found that the reduction of NO_x

68 emission resulted in a decrease of nitrate in the NO_x-limited regime, and an increase

69 of nitrate under extreme conditions in the VOC-limited regime. Despite that, the

70 single-site box model results could not distinguish the regional differences among

71 chemical regimes; the basic hypotheses in box models to predict nitrate production,

72 e.g., stagnant atmosphere or fixed NO_2/NO_y ratio, are also unreasonable in the real

73 atmosphere.

74   As an important precursor for both fine particles and ozone, the strict control of

75 NO_x emission has started in China since the 12th Five-Year Plan (Zheng et al., 2018).

76 A confounding factor is that, for most cities in China, the production of O_3 is usually

77 limited by VOC_s (Liu et al., 2010). The control of NO_x emission has therefore

78 resulted in an increase of O_3 concentrations in recent years (Li et al., 2021a; Li et al.,

79 2019a; Kalsoom et al., 2021), implying complex impacts on nitrate formation. Some

80 simulations thought that the NO_x emission increase in 2005–2012 resulted in an

81 increase of nitrate by 3.4% yr^{-1} in eastern China (Geng et al., 2017; Wang et al.,

82 2013), and the following NO_x emission control resulted in a decrease of nitrate by 3–

83 14% (Wang et al., 2014). Recent evidence from field observations (Fu et al., 2020)

84 and numerical simulations (Dong et al., 2014) suggested that the NO_x emission

85   reduction in China could result in an increase of nitrate in winter through increased

86   photochemical oxidants and nocturnal N_2O_5 chemistry, but a decrease in other seasons.

87   In the next 5–10 years, SO_2 emissions might level off in China, while NO_x emissions

88   will become stringently controlled to ensure further air quality improvements (Zheng

89   et al., 2018). Accurately understanding the nonlinear aerosol and photochemistry

90   feedbacks is crucial to resolve the emerging nitrate pollution and to establish

91   reasonable air pollution control strategies in China.

92   To address this issue, we use comprehensive measurements and a regional

93   meteorology-chemistry model combined with hypothetical NO_x emission scenarios to

94   establish the nonlinear response relationships between particulate nitrate and NO_x

95   emission controls in the megalopolises of China. The model configurations, numerical

96   designs and observational data are presented in Sect. 2. Sect. 3 discusses the results.

97   Finally, a summary is presented in Sect. 4.

98   **2 Materials and Methods**

99   **2.1 Model setup and experimental designs**

100   This study uses the Weather Research and Forecasting-Chemistry (WRF-Chem)

101   model version 4.1 developed by Grell et al. (2002) to simulate the meteorology and

102   atmospheric chemistry. The mesoscale meteorology and air quality simulations of

103   WRF-Chem have been improved in terms of incorporating the satellite-derived land

104   surface parameters (Li et al., 2014; Li et al., 2017), and optimizing the SIA formation

105   pathways enhanced by mineral aerosols (Li et al., 2019b; Huang et al., 2014b).

106   The modeling domain covers two main megalopolises of China and its adjacent

107   areas—the Beijing-Tianjin-Hebei (BTH) region and the Yangtze River Delta (YRD)

108   region (Fig. 1). The modeling framework is configured with 81×86 grid cells at 25 km

109   horizontal resolution. The model is run with an 84-hour model cycle, with the first 12

110   hours discarded as spin-up time and model outputs of each model cycle to provide

111   chemical initial conditions for the subsequent overlapping 84-hour simulation. The 6-

112   hour, 1°×1° National Centers for Environmental Prediction Final (NCEP/FNL)

113   analysis fields are regularly input for the model initial and lateral boundary

114   meteorological conditions.

115   The model physical configurations include the YSU boundary layer scheme

116   (Noh et al., 2003), the RRTMG radiation scheme (Iacono et al., 2008), the Noah land

117   surface scheme (Ek et al., 2003) and the Lin microphysics scheme (Lin et al., 1983).

118   We have further updated the land cover type and vegetation data in WRF mesoscale

119   model with the latest land surface parameters derived from Moderate Resolution

120   Imaging Spectroradiometer (Li et al., 2014; Li et al., 2017).

121   The atmospheric chemistry is simulated using the Carbon Bond Mechanism

122   version Z (CBMZ) (Zaveri and Peters, 1999) gas-phase chemistry module coupled

123   with a four-bin sectional Model for Simulating Aerosol Interactions and Chemistry

124   (MOSAIC) (Zaveri et al., 2008). The aqueous-phase chemistry is based on the

125   Carnegie Mellon University (CMU) scheme including 50 species and more than 100

126   reactions (Fahey and Pandis, 2001). Formation of SIA in the model accounts for the

127   gas-phases oxidation of SO_2 and NO_2, and aqueous-phase oxidation of SO_2 by

128   hydrogen peroxide (H_2O_2) and O_3 in cloud. We have also optimized the SIA

129   formation pathways by including the aqueous SO_2 oxidation catalyzed by mineral

130   ions and heterogeneous uptake of SO_2, NO_2, NO_3, N_2O_5 and HNO_3 on mineral

131   aerosols in the MOSAIC aerosol module (Li et al., 2019b; Huang et al., 2014b).

132   Anthropogenic emissions are adopted from the 2016 Multi-resolution Emission

133   Inventory for China (MEIC) and the 2010 MIX-Asia emission inventory for regions

134   outside of mainland China developed by Tsinghua University (http://meicmodel.org).

135 Biogenic emissions are calculated online using the Model of Emissions of Gases and

136 Aerosols from Nature (Guenther et al., 2006).

137   A series of WRF-Chem simulations are designed as summarized in Table 1. In

138 the baseline simulation (denoted as the B0 scenario), the anthropogenic emissions in

139 China remain unchanged at the usual levels. Simulation N0 is the same as the base

140 case B0, but it only considers the NO_2+OH gas-phase oxidation pathway for the

141 production of nitrate aerosol. The B0 and N0 simulations are designed to distinguish

142 the formation mechanisms for the high concentrations of nitrate aerosols during the

143 warm and cold seasons. A group of sensitivity scenarios (C1~C8) are designed with

144 the perturbed anthropogenic NO_x emissions in China cut by 10%, 20%...and 80%,

145 respectively. The differences between B0 and C1~C8 simulations are calculated to

146 illustrate the responses of particulate pollution in China's megacities to the NO_x

147 emission reduction scenarios. Another simulation (E1) is designed with the

148 anthropogenic emission of NO_x in China set to the 2012 level to show the impacts of

149 2012–2016 NO_x control strategy on particulate pollution.

150   For all simulation scenarios, two month-long periods during the Campaign on

151 Air Pollution and Urban Meteorology in Yangtze River Delta (CAPUM-YRD)—

152 August 15 to September 16 (Period I) and November 24 to December 26 (Period II) in

153 2016, are simulated to represent the warm and cold seasons, respectively (Shu et al.,

154 2019). The complete simulation consists of thirteen 84-hour model cycles with the

155 first 6 days as spin-up for chemistry and the remaining model outputs for analysis.

156 **2.2 Weather and air pollutants data**

157   Surface meteorological observations at 186 land-based automatic stations in

158 China (Fig. 1) are collected for model meteorological validation, including hourly

159   data of 2 m air temperature, 2 m relative humidity and 10 m wind speed. These data

160   are archived at the U. S. National Climatic Data Center (NCDC) (Smith et al., 2011).

161   Air pollutants data at the national air quality monitoring network and regional

162   supersites of China (Fig. 1) are used for model chemical validation. Six routine air

163   pollutants including particulate matter with aerodynamic diameter less than 10 µm

164   (PM_{10}), $PM_{2.5}$, SO_2, NO_2, carbon monoxide (CO) and O_3 are monitored and reported

165   hourly by Chinese National Environmental Monitoring Center (CNEMC) network

166   (available at http://websearch.mep.gov.cn/). This nationwide monitoring network

167   includes 1597 sites covering 454 cities in mainland China, as shown in Fig. 1.

168   Additionally, four comprehensive atmospheric environment supersites in YRD

169   including Dianshanhu (DSH; 31.1ºN, 121.0°E), Pudong (PD; 31.2º N, 121.5°E),

170   Nanjing (NJ; 32.1ºN, 118.8°E) and Hangzhou (HZ; 30.3ºN, 120.2°E) measured the

171   mass concentrations of $PM_{2.5}$, water-soluble ions (sulfate, nitrate, ammonium, sodium,

172   chloride, potassium, calcium and magnesium), carbonaceous aerosols (elemental

173   carbon (EC) and organic carbon (OC)) and gaseous pollutants (SO_2, NO_2, CO and O_3)

174   during the CAPUM-YRD campaign. Details for the methods and data at the four

175   supersites are described in Shu et al. (2019).

176   **3 Results and discussions**

177   **3.1 Model weather and chemical validation**

178   Model evaluations indicate that the WRF-Chem model is able to simulate the

179   weather and atmospheric pollution characteristics in China. The simulated magnitudes

180   of surface temperature by WRF-Chem in general agree with actual observations, with

181   a correlation efficient (R) of 0.89 and 0.94, and a normalized mean bias (NMB) of

182   −0.55% and −0.80% respectively in Period I and Period II (Table 2). Underestimation

183   of relative humidity (−5.65% in Period I and −6.56% in Period II) is common in the

184   WRF simulation and is attributed to the influence of the boundary layer

185   parameterization on the weather forecast (Bhati and Mohan, 2018; Gomez-Navarro et

186   al., 2015). Clear overestimation of wind speed (23.72% in Period I and 40.64% in

187   Period II) might be because of the unresolved topography in WRF (Jimenez et al.,

188   2013; Li et al., 2014).

189   The predicted concentrations of routine air pollutants also faithfully captures the

190   spatial and seasonal patterns of observed surface $PM_{2.5}$, SO_2, NO_2 and O_3 levels in

191   both seasons (Fig. 2). Both simulations and observations display high air pollutant

192   concentrations in the vicinity of North China Plain (NCP) and eastern China, but with

193   higher O_3 levels in the warm seasons and oppositely higher $PM_{2.5}$ and other gaseous

194   pollutants in winter. The model statistical evaluations show a MB of −3.66, −1.14, 4.7

195   and 18.32 μg m^{-3}, and NMB of −9.92, −6.46, 16.47 and 7.72% for $PM_{2.5}$, SO_2, NO_2

196   and O_3 in Period I, and a relatively larger MB of −27.31, −11.65, 1.27 and −39.01 μg

197   m^{-3}, and NMB of −29.82, −28.11, 2.40 and −31.05% in Period II, respectively (Table

198   3). The uncertainty in emissions data, the absence of secondary organic aerosol in

199   MOSAIC aerosol chemistry or the simulated wind errors may be responsible for the

200   larger atmospheric chemical biases in winter, which has been extensively discussed in

201   some studies (Zhao et al., 2016; Li et al., 2021a).

202   As the most important component of $PM_{2.5}$, reasonable representation of SIA is

203   imperative to $PM_{2.5}$ simulation. Evaluations with measurements of $PM_{2.5}$ components

204   at the four supersites of eastern China show that the model performs reasonably in

205   simulating the seasonal variations and proportions of aerosol species in $PM_{2.5}$, but it is

206   biased low by 10–40% in simulating the magnitudes of SIA concentrations (Fig. 3).

207   The model underestimation is −1.8, −2.2 and −2.2 μg m^{-3} for sulfate, nitrate and

208   ammonium, respectively, in Period I, and −2.6, −4.3 and −3.4 μg m^{-3} in Period II. The

209   model also captures the large change of S/N ratios from the warm to cold seasons, that

210   vary from 2.4 in Period I to 0.6 in Period II. Our previous work (Li et al., 2019) has

211   confirmed that the optimized aqueous and heterogeneous SIA formation pathways in

212   WRF-Chem significantly reduce the model biases by 41.38% for sulfate and 44.55%

213   for nitrate during the CAPUM-YRD campaign of 2016. Recent studies highlighted

214   that the remaining SIA simulation biases may be attributed to the missing aqueous

215   oxidation of SO_2 by NO_2 on alkaline aerosols under humid conditions (Wang et al.,

216   2016; Cheng et al., 2016).

3.2 Air pollution and aerosol composition characteristics

218   Chemical composition analyses of major gaseous and particulate air pollutants

219   suggest large seasonal variations of air pollution characteristics in China (Fig. 2).

220   Mainly emitted from combustion sources, atmospheric pollutants accumulate in the

221   densely industrialized and populated megalopolises of China, with a hotspot along

222   Beijing, Hebei, Shandong and their adjacent cities frequently exceeding China's

223   National Ambient Air Quality Standards. The average concentrations of $PM_{2.5}$, SO_2,

224   NO_2 and daily-maximum O_3 in China's routine air quality monitoring network are

225   36.88, 17.65, 28.53 and 237.45 $\mu g\ m^{-3}$ for Period I, and 91.59, 41.45, 53.01 and

226   125.62 $\mu g\ m^{-3}$ for Period II. The $PM_{2.5}$, SO_2 and NO_2 concentrations show obvious

227   increases by 148.35%, 134.84% and 85.80% during winter. The maximum $PM_{2.5}$

228   concentration recorded in the winter period could be more than 600 $\mu g\ m^{-3}$, which is

229   the highest value ever recorded in 2016 and leads to the "orange" air quality alert.

230   The further analyses of $PM_{2.5}$ mass concentrations, major $PM_{2.5}$ components and

231   gases at the four supersites in YRD are presented in Fig. 4–5. Organic matter (OM) is

232   obtained by multiplying the OC concentrations by a factor of 1.6, accounting for the

233   hydrogen and oxygen in organic compounds. The measured SIA concentrations

234   exhibit high levels, with average values of 18.8 μg m^{-3} for Period I and 37.1 μg m^{-3}

235   for Period II. The three SIA components together account for 48.6% and 56.9% of the

236   total PM$_{2.5}$ mass concentrations, and become the dominant components of PM$_{2.5}$ in

237   the two periods. The ratios of sulfate, nitrate and ammonium in total PM$_{2.5}$ range from

238   13.5–28.9%, 9.4–15.5% and 9.4–14.9% at the four supersites for Period I, and 9.2–

239   20.3%, 11.5–32.1% and 7.0–19.8% for Period II, respectively. The higher proportion

240   of nitrate in PM$_{2.5}$ than that of sulfate during winter, with a sulfur/nitrogen (S/N) ratio

241   of 0.64, is in accordance with recent observations during other winter haze periods in

242   China (Shao et al., 2018; Zhang et al., 2018; Zhang et al., 2019). They emphasized

243   that since the enactment of Clean Air Action Plan in 2013, the PM$_{2.5}$ components had

244   changed clearly with decreasing contributions from coal combustion.

245   The high proportions of sulfate and nitrate in PM$_{2.5}$ could be related to the high

246   oxidation rates of SO$_2$ and NO$_2$. The observed average values of sulfur oxidation ratio

247   (SOR=[SO$_4^{2-}$]/([SO$_4^{2-}$]+[SO$_2$])) and nitrogen oxidation ratio (NOR=[NO$_3^-$]/([NO$_3^-$

248   ]+[NO$_2$])) are 0.41 and 0.13 in Period I, and 0.33 and 0.21 in Period II, indicating

249   enhanced secondary oxidation formation. Figure 6 illustrates the contributions of each

250   formation pathway for the high concentrations of nitrate calculated from B0 and E0

251   simulations. It is shown that on a daily basis the gas-phase oxidation production of

252   HNO$_3$ and its subsequent partitioning to the aerosol phase is the principal formation

253   route for particulate nitrate, with the average contributions of 60.19% for BTH and

254   91.71% for YRD in Period I and 75.14% for BTH and 85.94% for YRD in Period II,

255   heterogeneous hydrolysis of N$_2$O$_5$ and other reactive nitrogen gases contributed to the

256   remaining nitrate particularly in BTH with high aerosol loading. These results are in

257   line with previous assessments (Alexander et al., 2009; Wen et al., 2018; Sun et al.,

258   2018), which reported that the global tropospheric nitrate burden is dominated by

259   nitrate formation via NO_2+OH (76%), followed by N_2O_5 hydrolysis (18%).

3.3 Nonlinear responses of $PM_{2.5}$ to NO_x emissions and their policy implication

3.3.1 $PM_{2.5}$-NO_x and O_3-NO_x responses in the warm and cold seasons

262   NO_x is key in atmospheric chemistry and serves as an important precursor for

263   both ozone and secondary aerosols. We conduct a series of simulations with perturbed

264   NO_x emissions (−10%~−80%) to assess the responses of $PM_{2.5}$ mass concentrations to

265   NO_x emissions in two megalopolises of China (Fig. 7). The WRF-Chem simulation

266   results show that the responses of surface $PM_{2.5}$ concentrations to NO_x emissions vary

267   in different seasons and display strong nonlinear in winter. To better quantify their

268   effectiveness, we define the NO_x emission control efficiency (β), denoting the

269   percentage change of $PM_{2.5}$ or its components concentrations in response to

270   successive 10% cut of NO_x emission. In Period I (Aug–Sep), the $PM_{2.5}$-NO_x responses

271   are closer to a linear function, reflecting a stronger sensitivity to NO_x emission

272   changes in the warm season. The surface $PM_{2.5}$ concentrations decrease almost

273   linearly as we gradually reduce NO_x emissions in China, with the β values of −2.65%

274   in BTH and −2.79% in YRD. However, the $PM_{2.5}$-NO_x emission responses in Period

275   II (Nov–Dec) display strong nonlinearity and are analogous to a bell-shaped

276   distribution for both regions. The NO_x emission reduction within the first 50% would

277   even increase surface mean $PM_{2.5}$ concentrations by +1.33% in BTH, and this β value

278   increases to +1.42% in YRD with the first 40% NO_x emission reduction.

279   Subsequently, the $PM_{2.5}$ responses shift towards a similar linear pattern, with a β

280   value of −3.47% in BTH and −3.89% in YRD.

281   The distinct forms of $PM_{2.5}$-NO_x emission responses in the warm and cold

282   seasons are determined by the changing features of SIA concentrations in response to

283   NO_x controls (Fig. 8–9) under the seasonal ozone chemical sensitivity regimes. The

284   photochemical indicator of $\Delta[O_3]_{NO_x}/\Delta[O_3]_{VOC_s}$ with a critical value of 1.0 is used to

285   investigate the season-varying ozone sensitivity in China, which is calculated as the

286   ratio of ozone concentration changes under 20% NO_x emission reduction to that under

287   20% VOC_s emission reduction (Fig. S1). The results indicate a strong VOC-limited

288   ozone chemistry across China during winter, while either VOC-limited regime over a

289   large portion of NCP and eastern China or NO_x-limited regime in northern and

290   western China during summer-autumn, as also indicated from previous studies (Xie et

291   al., 2014; Dong et al., 2014; Liu et al., 2010). We find larger O_3 and OH productions

292   under lower NO_x emission conditions in both seasons, particularly in Period II (Nov–

293   Dec) with an increase rate of 28.51% and 36.92% in BTH and 34.36% and 33.6% in

294   YRD per 10% cut of NO_x emission than the base case (Fig. 8–9(b, d)). The SIA

295   formation chemistry is highly limited by atmospheric oxidants produced from the

296   NO_x-VOC_s-O_3 photochemical cycles. The nonlinear O_3-NO_x responses indicate a

297   rather complicated aerosol and photochemistry feedback in megacities.

298   **3.3.2 Nonlinear responses of particulate nitrate to NO_x emissions**

299   The SIA formation chemistry is basically driven by atmospheric oxidants levels,

300   and a reduction of NO_x emission may have counter-intuitive effects on SIA

301   components by controlling atmospheric oxidants levels. The calculated SIA

302   components for each emission scenario in both months show that sulfate has minor

303   changes with reducing NO_x emissions but nitrate and ammonium aerosols can be

304   substantially decreased/increased (Fig. 8–9).

305   Response of sulfate to the NO_x emissions is more predictable and determined by

306   the changes of atmospheric oxidant levels since that the conversion of SO_2 to sulfate

307   is mainly driven by OH in the gas-phase and by dissolved H_2O_2 or O_3 in the presence

308 of fog or cloud. In Period I (Aug–Sep), the sulfate-NO_x response follows a bell-

309 shaped distribution as that of O_3-NO_x response curve, with a fitted curve in Eq. 1. The

310 surface sulfate concentrations has minor changes by −6.69%~+2.33% in BTH and by

311 −9.55%~+3.47% in YRD under the −10~−80% NO_x emission reduction scenarios.

$$312 \qquad [SO_4^{2-}]=-2.45\Delta E_{NOx}^2-2.15\Delta E_{NOx}+5.90 \text{ in BTH} \qquad (Eq. 1)$$

$$313 \qquad [SO_4^{2-}]=-2.26\Delta E_{NOx}^2-1.31\Delta E_{NOx}+6.65 \text{ in YRD}$$

314 where $[SO_4^{2-}]$ is the surface mean concentration of sulfate ($\mu g\ m^{-3}$); ΔE_{NOx} is the

315 percentage change of NO_x emission (%).

316 As expected, the production of nitrate reflects a strong sensitivity to NO_x and it

317 decreases linearly with the NO_x emission control, with a β value of −10.89% in BTH

318 and −11.39% in YRD, which further leads to a decrease of ammonium concentrations

319 by −4.10% in BTH and −4.73% in YRD. The formation of nitrate involves the

320 $NO_2+OH \rightarrow HNO_3$ gas-phase oxidation and the heterogeneous hydrolysis of N_2O_5.

321 The strong sensibility of particulate nitrate in response to NO_x decrease can be

322 explained by its synchronously suppressive production of intermediate products

323 HNO_3 and N_2O_5. For example, when the NO_x emission is cut by 20%, the surface

324 NO_2 concentration in BTH drops by 21.96% but O_3 increases slightly by 2.56% due to

325 greater VOC availability in warm season, leading to substantial reductions in the

326 surface HNO_3 (−16.72%) and N_2O_5 (−8.94%) concentrations.

327 In Period II (Nov–Dec), we find opposite results with bell-shaped distributions

328 for nitrate-NO_x response (Eq. 2) and ammonium-NO_x response (Eq. 3), and linearly

329 increasing sulfate concentrations (β=+1.34% in BTH and +2.29% in YRD) in the

330 VOC-poor environment, leading to small $PM_{2.5}$ changes in winter. Such nonlinear

331 nitrate-NO_x emission responses can be explained by the derived excess oxidants as we

332 gradually reduce NO_x emissions in each scenario. It is noted that in winter the nitrate-

333   NO_x response is determined by the production of N_2O_5 intermediate product, which is

334   more sensitive to the concentration of atmospheric oxidants under low NO_x emission

335   reduction conditions. The significant increase of surface O_3 in each NO_x emission

336   scenario leads to an enhancement of N_2O_5 level from 10% to more than 100%, which

337   is produced from the $NO_2 \xrightarrow{O_3} NO_3 \xrightarrow{NO_2} N_2O_5$ chemical reaction and is a crucial intermediate

338   product for nitrate formation. In spite of the HNO_3 concentration remaining nearly

339   unchanged or decreasing slightly by less than 5% in response to NO_x control, nitrate

340   is found to increase (β=+4.28% in BTH and +4.60% in YRD) with higher N_2O_5

341   produced from the increased ozone introduced by attenuated titration. An inflexion

342   point appears at the 40–50% NO_x emission reduction scenario, and a further reduction

343   in NO_x emission is predicted to cause −8.74% and −6.18% reductions of particulate

344   nitrate and ammonium for BTH, and −10.59% and −8.17% for YRD.

345   $$[NO_3^-]=-34.54\Delta E_{NOx}^2-30.66\Delta E_{NOx}+10.52 \text{ in BTH} \qquad \text{(Eq. 2)}$$

346   $$[NO_3^-]=-36.53\Delta E_{NOx}^2-26.94\Delta E_{NOx}+9.70 \text{ in YRD}$$

347   $$[NH_4^+]=-9.12\Delta E_{NOx}^2-8.73\Delta E_{NOx}+5.40 \text{ in BTH} \qquad \text{(Eq. 3)}$$

348   $$[NH_4^+]=-10.55\Delta E_{NOx}^2-8.36\Delta E_{NOx}+4.58 \text{ in YRD}$$

349   where $[NO_3^-]$ and $[NH_4^+]$ are the surface mean concentrations ($\mu g\ m^{-3}$) of nitrate

350   and ammonium, respectively.

351   These results reveal that the increase in atmospheric oxidants in response to NO_x

352   control can offset the decreasing precursor concentrations and further enhance the

353   formation of secondary nitrate, as recently found during the COVID-19 pandemic

354   (Huang et al., 2020; Li et al., 2021b). Our results provide insights for developing

355   mitigation strategies for the ubiquitous secondary aerosols in winter haze of China.

3.3.3 Impacts of 2012–2016 NO$_x$ control strategy on particulate pollution

356

357   During the 12th Five-Year Plan period (2011–2015), a series of end-of-pipe

358 pollutant controls (e.g., Selective Catalytic Reduction techniques) were carried out for

359 power, industry and transportation sectors. These measures effectively controlled the

360 national NO$_x$ emissions by 22.8% from 2012 to 2016 (MEIC v1.3) in China. To

361 quantify the effects of recent NO$_x$ control measures on the levels of photochemical

362 oxidants and particulate nitrate, we conduct an additional simulation with NO$_x$

363 emissions set to the levels of 2012 in E1.

364   The model simulations (Fig. 10) suggest that reducing China's NO$_x$ emissions

365 alone from 2012 to 2016 leads to an average −24.93%~−8.62% decrease of NO$_x$

366 concentrations in the surface layer. As previously pointed out, the 2012–2016 NO$_x$

367 emission control measures lead to increased O$_3$ and OH levels in winter, which offset

368 the effectiveness of NO$_x$ emission reduction in alleviating winter nitrate. No obvious

369 declines in the winter nitrate levels are observed and even increase in some areas

370 (+8.82% in BTH and 14.41% in YRD; Fig. S2–S3). As shown, the largest PM$_{2.5}$

371 responses shift towards the southern Hebei and central China provinces, where the

372 wintertime PM$_{2.5}$ concentrations are particularly high in this region. The substantial

373 emission changes from 2012 to 2016 lower the PM$_{2.5}$ air pollution by up to −1.84% in

374 BTH and −3.52% in YRD for Period I and oppositely increase PM$_{2.5}$ by 2.36% in

375 BTH and 4.67% in YRD for Period II. The past NO$_x$ emission control strategy leads

376 to increased atmospheric oxidant levels and deteriorate particulate pollution in winter

377 due to the nonlinear photochemistry and aerosol chemical feedbacks, without regard

378 to the other control measures. This conclusion is also supported by evidence from the

379 recent field observations (Fu et al., 2020).

4 Conclusions

380

381   Recent air pollution actions have significantly lowered the $PM_{2.5}$ levels in China

382   via controlling emissions of SO_2 and NO_x, but raised a new question of how effective

383   NO_x emission controls can be on the mitigation of emerging nitrate and ozone air

384   pollution. We use comprehensive measurements and a regional meteorology-

385   chemistry model with optimized mechanisms to establish the nonlinear responses

386   between particulate nitrate and NO_x emission controls in the megalopolises of China.

387   Nitrate is an essential component of $PM_{2.5}$ in eastern China, accounting for 9.4–

388   15.5% and 11.5–32.1% of the total $PM_{2.5}$ mass for the warm and cold seasons,

389   respectively. We find that the efficiency of $PM_{2.5}$ reduction is highly sensitive to NO_x

390   emission and it varies in different seasons depending on the ozone chemical regimes.

391   The reduction of NO_x emissions during summer-autumn results in almost linearly

392   lower $PM_{2.5}$ by −2.65% in BTH and −2.79% in YRD per 10% cut of NO_x emissions,

393   whereas it increases the atmospheric oxidant levels (28.51% and 36.92% for O_3 and

394   OH in BTH and 34.36% and 33.6% in YRD) and leads to a rather complicated

395   response of the PM components in winter. Nitrate is found to increase (β=+4.28% in

396   BTH and +4.60% in YRD) in winter with higher N_2O_5 intermediate produced from

397   the increased ozone introduced by attenuated titration, despite the nearly unchanged

398   or slightly decreased HNO_3 concentrations in response to NO_x control. An inflexion

399   point appears at 40–50% NO_x emission reduction, and a further reduction of NO_x

400   emission is predicted to cause −8.74% reductions of particulate nitrate for BTH and

401   −10.59% for YRD. In addition, the 2012–2016 NO_x emission control strategy leads to

402   −24.93%~−8.62% decrease of surface NO_x, and no change or even increase of

403   wintertime nitrate in BTH (+8.82%) and YRD (14.41%).

404   Our results emphasize that future $PM_{2.5}$ pollution mitigation strategies should

405   also focus on reducing the key oxidants involved in secondary aerosol production.

406   VOC_s, which is not a direct precursor for SIA, is effective in SIA controls due to their

407   influence on atmospheric oxidation cycles (Tsimpidi et al., 2008; Womack et al., 2019;

408   Nguyen and Dabdub, 2002). Womack et al. (2019) evaluated the impacts of

409   traditional ozone mitigation strategies on ammonium nitrate production in the Salt

410   Lake Valley, USA. They found that the ammonium nitrate aerosol pollution is

411   responsive to VOC_s control and not initially responsive to NO_x control. Tsimpidi et al.

412   (2008) also showed that the reduction of VOC_s emissions caused a marginal increase

413   of $PM_{2.5}$ during summer in eastern United States, whereas it resulted in a decrease of

414   oxidant levels and 5–20% reduction of both inorganic and organic $PM_{2.5}$ components

415   during winter. Larger and synchronized NO_x and VOC_s emissions reductions are

416   required to overcome the adverse effects of nonlinear photochemistry and aerosol

417   chemical feedbacks.

418   Atmospheric NH_3 also acts as a critical neutralizing species for SIA production

419   and efficient haze mitigation (Liu et al., 2019). Atmospheric chemistry modeling

420   indicated that controlling NH_3 emission would significantly reduce the population-

421   weighted $PM_{2.5}$ concentration by 6.2–21% with 60–100% NH_3 reductions in January,

422   implying the need to consider NH_3 emission controls when designing the $PM_{2.5}$

423   pollution mitigation strategies (Wen et al., 2021). China's anthropogenic emissions are

424   estimated to decrease by 62% for SO_2 and 17% for NO_x over 2010–2017, while

425   NH_3 emissions slightly increased by 1% (Zheng et al., 2018). The recent "Three-year

426   Action Plan Fighting for a Blue Sky" calls for agricultural NH_3 emission controls but

427   without a specific reduction target. Such emission changes would emphasize the need

428   to jointly consider multi-pollutants emissions controls for mitigating SIA air pollution.

429 **Author contribution**

430   Mengmeng Li developed the model code, designed the numerical experiments,

431 and wrote the original draft. Zihan Zhang carried out the numerical experiments. Shu

432 Li and Bingliang Zhuang validated and analyzed the model results. Tijian Wang and

433 Min Xie reviewed and revised the manuscript.

434 **Competing interests**

435   The authors declare that they have no conflict of interest.

436 **Acknowledgement**

437   This study is funded by the National Natural Science Foundation of China

438 (41975153, 42077192 and 41775056), the National Key Basic Research Development

439 Program of China (2019YFC0214603, 2020YFA0607802), and the Emory

440 University-Nanjing University Collaborative Research Grant.

441 **Data availability statement**

442   The   WRF-Chem   model   version   4.1   is   available   at

443 http://www2.mmm.ucar.edu/wrf/users/downloads.html. The NCEP FNL data are

444 accessible at the National Center for Atmospheric Research (NCAR) Research Data

445 Archive (RDA; http://rda.ucar.edu/datasets/ds083.2/). The MEIC anthropogenic

446 emission inventories are available at www.meicmodel.org, and for more information,

447 please contact Q. Zhang (qiangzhang@tsinghua.edu.cn). The surface weather data are

448 accessible at the Integrated Surface Database (https://www.ncdc.noaa.gov/isd/data-

449 access). The surface air pollutants and aerosol species data are provided by Chinese

450 National Environmental Monitoring Center (http://www.cnemc.cn/en/) and archived

451 at https://doi.org/10.6084/m9.figshare.12818807.v1.

References

Alexander, B., Hastings, M. G., Allman, D. J., Dachs, J., Thornton, J. A., and Kunasek, S. A.: Quantifying atmospheric nitrate formation pathways based on a global model of the oxygen isotopic composition (ΔO^{17}) of atmospheric nitrate, Atmos Chem Phys, 9, 5043-5056, 2009.

Bhati, S. and Mohan, M.: WRF-urban canopy model evaluation for the assessment of heat island and thermal comfort over an urban airshed in India under varying land use/land cover conditions, Geosci Lett, 5, doi: 10.1186/s40562-018-0126-7, 2018.

Cheng, Y. F., Zheng, G. J., Wei, C., Mu, Q., Zheng, B., Wang, Z. B., Gao, M., Zhang, Q., He, K. B., Carmichael, G., Poschl, U., and Su, H.: Reactive nitrogen chemistry in aerosol water as a source of sulfate during haze events in China, Sci Adv, 2, doi: 10.1126/sciadv.1601530, 2016.

Dong, X. Y., Li, J., Fu, J. S., Gao, Y., Huang, K., and Zhuang, G. S.: Inorganic aerosols responses to emission changes in Yangtze River Delta, China, Sci Total Environ, 481, 522-532, 2014.

Ek, M. B., Mitchell, K. E., Lin, Y., Rogers, E., Grunmann, P., Koren, V., Gayno, G., and Tarpley, J. D.: Implementation of Noah land surface model advances in the National Centers for Environmental Prediction operational mesoscale Eta model, J Geophys Res-Atmos, 108, doi: 10.1029/2002jd003296, 2003.

Fahey, K. M. and Pandis, S. N.: Optimizing model performance: variable size resolution in cloud chemistry modeling, Atmos Environ, 35, 4471-4478, 2001.

Fu, X., Wang, T., Gao, J., Wang, P., Liu, Y. M., Wang, S. X., Zhao, B., and Xue, L. K.: Persistent heavy winter nitrate pollution driven by increased photochemical oxidants in northern China, Environ Sci Technol, 54, 3881-3889, 2020.

Geng, G. N., Zhang, Q., Tong, D., Li, M., Zheng, Y. X., Wang, S. W., and He, K. B.: Chemical composition of ambient $PM_{2.5}$ over China and relationship to precursor emissions during 2005-2012, Atmos Chem Phys, 17, 9187-9203, 2017.

Gomez-Navarro, J. J., Raible, C. C., and Dierer, S.: Sensitivity of the WRF model to PBL parametrisations and nesting techniques: evaluation of wind storms over complex terrain, Geosci Model Dev, 8, 3349-3363, 2015.

Grell, G. A., McKeen, S., Michalakes, J., Bao, J. W., Trainer, M., and Hsie, E. Y.: Real-time simultaneous prediction of air pollution and weather during the

485   Houston 2000 field experiment, Fourth Conference on Atmospheric Chemistry:
486   Urban, Regional And Global Scale Impacts Of Air Pollutants, 224-227, 2002.
487   Guenther, A., Karl, T., Harley, P., Wiedinmyer, C., Palmer, P. I., and Geron, C.:
488   Estimates of global terrestrial isoprene emissions using MEGAN (Model of
489   Emissions of Gases and Aerosols from Nature), Atmos Chem Phys, 6, 3181-
490   3210, 2006.
491   He, P. Z., Xie, Z. Q., Chi, X. Y., Yu, X. W., Fan, S. D., Kang, H., Liu, C., and Zhan,
492   H. C.: Atmospheric $\Delta O^{17}(NO_3^-)$ reveals nocturnal chemistry dominates nitrate
493   production in Beijing haze, Atmos Chem Phys, 18, 14465-14476, 2018.
494   Huang, R. J., Zhang, Y. L., Bozzetti, C., Ho, K. F., Cao, J. J., Han, Y. M.,
495   Daellenbach, K. R., Slowik, J. G., Platt, S. M., Canonaco, F., Zotter, P., Wolf, R.,
496   Pieber, S. M., Bruns, E. A., Crippa, M., Ciarelli, G., Piazzalunga, A.,
497   Schwikowski, M., Abbaszade, G., Schnelle-Kreis, J., Zimmermann, R., An, Z. S.,
498   Szidat, S., Baltensperger, U., El Haddad, I., and Prevot, A. S. H.: High secondary
499   aerosol contribution to particulate pollution during haze events in China, Nature,
500   514, 218-222, 2014a.
501   Huang, X., Song, Y., Zhao, C., Li, M. M., Zhu, T., Zhang, Q., and Zhang, X. Y.:
502   Pathways of sulfate enhancement by natural and anthropogenic mineral aerosols
503   in China, J Geophys Res-Atmos, 119, 14165-14179, 2014b.
504   Huang, X., Ding, A., Gao, J., Zheng, B., Zhou, D., Qi, X., Tang, R., Wang, J., Ren, C.,
505   Nie, W., Chi, X., Xu, Z., Chen, L., Li, Y., Che, F., Pang, N., Wang, H., Tong, D.,
506   Qin, W., Cheng, W., Liu, W., Fu, Q., Liu, B., Chai, F., Davis, S., Zhang, Q., and
507   He, K.: Enhanced secondary pollution offset reductioin of primary emissions
508   during COVID-19 lockdown in China, Natl Sci Rev, 1-9, 2020.
509   Iacono, M. J., Delamere, J. S., Mlawer, E. J., Shephard, M. W., Clough, S. A., and
510   Collins, W. D.: Radiative forcing by long-lived greenhouse gases: Calculations
511   with the AER radiative transfer models, J Geophys Res-Atmos, 113, doi:
512   10.1029/2008jd009944, 2008.
513   Jimenez, P. A., Dudhia, J., Gonzalez-Rouco, J. F., Montavez, J. P., Garcia-
514   Bustamante, E., Navarro, J., de Arellano, J. V. G., and Munoz-Roldan, A.: An
515   evaluation of WRF's ability to reproduce the surface wind over complex terrain
516   based on typical circulation patterns, J Geophys Res-Atmos, 118, 7651-7669,
517   2013.

518 Kalsoom, U., Wang, T. J., Ma, C. Q., Shu, L., Huang, C. W., and Gao, L. B.:
519 Quadrennial variability and trends of surface ozone across China during 2015-
520 2018: A regional approach, Atmos Environ, 245, doi:
521 10.1016/j.atmosenv.2020.117989, 2021.

522 Li, K., Jacob, D. J., Liao, H., Shen, L., Zhang, Q., and Bates, K. H.: Anthropogenic
523 drivers of 2013-2017 trends in summer surface ozone in China, P Natl Acad Sci
524 USA, 116, 422-427, 2019a.

525 Li, M. M., Song, Y., Huang, X., Li, J. F., Mao, Y., Zhu, T., Cai, X. H., and Liu, B.:
526 Improving mesoscale modeling using satellite-derived land surface parameters in
527 the Pearl River Delta region, China, J Geophys Res-Atmos, 119, 6325-6346,
528 2014.

529 Li, M. M., Wang, T. J., Shu, L., Qu, Y. W., Xie, M., Liu, J. N., Wu, H., and Kalsoom,
530 U.: Rising surface ozone in China from 2013 to 2017: A response to the recent
531 atmospheric warming or pollutant controls?, Atmos Environ, 246, doi:
532 10.1016/j.atmosenv.2020.118130, 2021a.

533 Li, M. M., Wang, T. J., Xie, M., Zhuang, B. L., Li, S., Han, Y., Song, Y., and Cheng,
534 N. L.: Improved meteorology and ozone air quality simulations using MODIS
535 land surface parameters in the Yangtze River Delta urban cluster, China, J
536 Geophys Res-Atmos, 122, 3116-3140, 2017.

537 Li, M. M., Wang, T. J., Xie, M., Li, S., Zhuang, B. L., Huang, X., Chen, P. L., Zhao,
538 M., and Liu, J. E.: Formation and evolution mechanisms for two extreme haze
539 episodes in the Yangtze River Delta region of China during winter 2016, J
540 Geophys Res-Atmos, 124, 3607-3623, 2019b.

541 Li, M. M., Wang, T. J., Xie, M., Li, S., Zhuang, B. L., Fu, Q. Y., Zhao, M., Wu, H.,
542 Liu, J., Saikawa, E., and Liao, K.: Drivers for the poor air quality conditions in
543 North China Plain during the COVID-19 outbreak, Atmos Environ, 246, doi:
544 10.1016/j.atmosenv.2020.118103, 2021b.

545 Lin, Y. L., Farley, R. D., and Orville, H. D.: Bulk parameterization of the snow field
546 in a cloud model, J Clim Appl Meteorol, 22, 1065−1092, 1983.

547 Liu, M. X., Huang, X., Song, Y., Tang, J., Cao, J. J., Zhang, X. Y., Zhang, Q., Wang,
548 S. X., Xu, T. T., Kang, L., Cai, X. H., Zhang, H. S., Yang, F. M., Wang, H. B.,
549 Yu, J. Z., Lau, A. K. H., He, L. Y., Huang, X. F., Duan, L., Ding, A. J., Xue, L.
550 K., Gao, J., Liu, B., and Zhu, T.: Ammonia emission control in China would

551   mitigate haze pollution and nitrogen deposition, but worsen acid rain, P Natl

552   Acad Sci USA, 116, 7760-7765, 2019.

553   Liu, X. H., Zhang, Y., Xing, J., Zhang, Q. A., Wang, K., Streets, D. G., Jang, C.,

554   Wang, W. X., and Hao, J. M.: Understanding of regional air pollution over China

555   using CMAQ, part II. Process analysis and sensitivity of ozone and particulate

556   matter to precursor emissions, Atmos Environ, 44, 3719-3727, 2010.

557   Meng, Z., Dabdub, D., and Seinfeld, J. H.: Chemical coupling between atmospheric

558   ozone and particulate matter, Science, 277, 116-119, 1997.

559   Nguyen, K. and Dabdub, D.: NO_x and VOC control and its effects on the formation of

560   aerosols, Aerosol Sci Tech, 36, 560-572, 2002.

561   Noh, Y., Cheon, W. G., Hong, S. Y., and Raasch, S.: Improvement of the K-profile

562   model for the planetary boundary layer based on large eddy simulation data,

563   Bound-Lay Meteorol, 107, 401−427, 2003.

564   Pathak, R. K., Wang, T., and Wu, W. S.: Nighttime enhancement of $PM_{2.5}$ nitrate in

565   ammonia-poor atmospheric conditions in Beijing and Shanghai: Plausible

566   contributions of heterogeneous hydrolysis of N_2O_5 and HNO_3 partitioning,

567   Atmos Environ, 45, 1183-1191, 2011.

568   Pun, B. K. and Seigneur, C.: Sensitivity of particulate matter nitrate formation to

569   precursor emissions in the California San Joaquin Valley, Environ Sci Technol,

570   35, 2979-2987, 2001.

571   Seinfeld, J. H. and Pandis, S. N.: Atmospheric chemistry and physics: from air

572   pollution to climate change. 2nd Edition, John Wiley and Sons, Hoboken, NJ,

573   2006.

574   Shao, P. Y., Tian, H. Z., Sun, Y. J., Liu, H. J., Wu, B. B., Liu, S. H., Liu, X. Y., Wu,

575   Y. M., Liang, W. Z., Wang, Y., Gao, J. J., Xue, Y. F., Bai, X. X., Liu, W., Lin, S.

576   M., and Hu, G. Z.: Characterizing remarkable changes of severe haze events and

577   chemical compositions in multi-size airborne particles (PM_1, $PM_{2.5}$ and PM_{10})

578   from January 2013 to 2016-2017 winter in Beijing, China, Atmos Environ, 189,

579   133-144, 2018.

580   Shu, L., Wang, T., Xie, M., Li, M., Zhao, M., Zhang, M., and Zhao, X.: Episode study

581   of fine particle and ozone during the CAPUM-YRD over Yangtze River Delta of

582   China: characteristics and source attribution, Atmos Environ, 203, 87-101, 2019.

583   Silver, B., Reddington, C. L., Arnold, S. R., and Spracklen, D. V.: Substantial
584   changes in air pollution across China during 2015-2017, Environ Res Lett, 14,
585   114012, 2018.

586   Smith, A., Lott, N., and Vose, R.: The Integrated Surface Database Recent
587   Developments and Partnerships, B Am Meteorol Soc, 92, 704-708, 2011.

588   Sun, P., Nie, W., Chi, X. G., Xie, Y. N., Huang, X., Xu, Z., Qi, X. M., Xu, Z. N.,
589   Wang, L., Wang, T. Y., Zhang, Q., and Ding, A. J.: Two years of online
590   measurement of fine particulate nitrate in the western Yangtze River Delta:
591   influences of thermodynamics and N_2O_5 hydrolysis, Atmos Chem Phys, 18,
592   17177-17190, 2018.

593   Tsimpidi, A. P., Karydis, V. A., and Pandis, S. N.: Response of fine particulate matter
594   to emission changes of oxides of nitrogen and-anthropogenic volatile organic
595   compounds in the eastern United States, J Air Waste Manage, 58, 1463-1473,
596   2008.

597   Wang, G. H., Zhang, R. Y., Gomez, M. E., Yang, L. X., Zamora, M. L., Hu, M., Lin,
598   Y., Peng, J. F., Guo, S., Meng, J. J., Li, J. J., Cheng, C. L., Hu, T. F., Ren, Y. Q.,
599   Wang, Y. S., Gao, J., Cao, J. J., An, Z. S., Zhou, W. J., Li, G. H., Wang, J. Y.,
600   Tian, P. F., Marrero-Ortiz, W., Secrest, J., Du, Z. F., Zheng, J., Shang, D. J.,
601   Zeng, L. M., Shao, M., Wang, W. G., Huang, Y., Wang, Y., Zhu, Y. J., Li, Y. X.,
602   Hu, J. X., Pan, B., Cai, L., Cheng, Y. T., Ji, Y. M., Zhang, F., Rosenfeld, D., Liss,
603   P. S., Duce, R. A., Kolb, C. E., and Molina, M. J.: Persistent sulfate formation
604   from London Fog to Chinese haze, P Natl Acad Sci USA, 113, 13630-13635,
605   2016.

606   Wang, J. D., Zhao, B., Wang, S. X., Yang, F. M., Xing, J., Morawska, L., Ding, A. J.,
607   Kulmala, M., Kerminen, V. M., Kujansuu, J., Wang, Z. F., Ding, D. A., Zhang,
608   X. Y., Wang, H. B., Tian, M., Petaja, T., Jiang, J. K., and Hao, J. M.: Particulate
609   matter pollution over China and the effects of control policies, Sci Total Environ,
610   584, 426-447, 2017.

611   Wang, S. X., Xing, J., Zhao, B., Jang, C., and Hao, J. M.: Effectiveness of national air
612   pollution control policies on the air quality in metropolitan areas of China, J
613   Environ Sci, 26, 13-22, 2014.

614   Wang, Y., Zhang, Q. Q., He, K., Zhang, Q., and Chai, L.: Sulfate-nitrate-ammonium
615   aerosols over China: response to 2000-2015 emission changes of sulfur dioxide,
616   nitrogen oxides, and ammonia, Atmos Chem Phys, 13, 2635-2652, 2013.

617   Wen, L., Xue, L. K., Wang, X. F., Xu, C. H., Chen, T. S., Yang, L. X., Wang, T.,
618   Zhang, Q. Z., and Wang, W. X.: Summertime fine particulate nitrate pollution in
619   the North China Plain: increasing trends, formation mechanisms and implications
620   for control policy, Atmos Chem Phys, 18, 11261-11275, 2018.

621   Wen, Z., Xu, W., Pan, X. Y., Han, M. J., Wang, C., Benedict, K., Tang, A. H., Collet,
622   J. L., and Liu, X. J.: Effects of reactive nitrogen gases on the aerosol formation
623   in Beijing from late autumn to early spring, Environ Res Lett, 16, doi:
624   10.1088/1748-9326/abd973, 2021.

625   Womack, C. C., McDuffie, E. E., Edwards, P. M., Bares, R., de Gouw, J. A.,
626   Docherty, K. S., Dube, W. P., Fibiger, D. L., Franchin, A., Gilman, J. B.,
627   Goldberger, L., Lee, B. H., Lin, J. C., Lone, R., Middlebrook, A. M., Millet, D.
628   B., Moravek, A., Murphy, J. G., Quinn, P. K., Riedel, T. P., Roberts, J. M.,
629   Thornton, J. A., Valin, L. C., Veres, P. R., Whitehill, A. R., Wild, R. J., Warneke,
630   C., Yuan, B., Baasandorj, M., and Brown, S. S.: An odd oxygen framework for
631   wintertime ammonium nitrate aerosol pollution in urban areas: NO_x and VOC
632   control as mitigation strategies, Geophys Res Lett, 46, 4971-4979, 2019.

633   Xie, M., Zhu, K. G., Wang, T. J., Yang, H. M., Zhuang, B. L., Li, S., Li, M. G., Zhu,
634   X. S., and Ouyang, Y.: Application of photochemical indicators to evaluate
635   ozone nonlinear chemistry and pollution control countermeasure in China,
636   Atmos Environ, 99, 466-473, 2014.

637   Xue, J., Yuan, Z. B., Lau, A. K. H., and Yu, J. Z.: Insights into factors affecting
638   nitrate in PM2.5 in a polluted high NO_x environment through hourly
639   observations and size distribution measurements, J Geophys Res-Atmos, 119,
640   4888-4902, 2014.

641   Zaveri, R. A. and Peters, L. K.: A new lumped structure photochemical mechanism
642   for large-scale applications, J Geophys Res-Atmos, 104, 30387-30415, 1999.

643   Zaveri, R. A., Easter, R. C., Fast, J. D., and Peters, L. K.: Model for Simulating
644   Aerosol Interactions and Chemistry (MOSAIC), J Geophys Res-Atmos, 113, doi:
645   10.1029/2007jd008782, 2008.

646   Zhai, S. X., Jacob, D. J., Wang, X., Shen, L., Li, K., Zhang, Y. Z., Gui, K., Zhao, T.
647   L., and Liao, H.: Fine particulate matter (PM$_{2.5}$) trends in China, 2013-2018:
648   separating contributions from anthropogenic emissions and meteorology, Atmos
649   Chem Phys, 19, 11031-11041, 2019.
650   Zhang, W. Q., Tong, S. R., Ge, M. F., An, J. L., Shi, Z. B., Hou, S. Q., Xia, K. H., Qu,
651   Y., Zhang, H. X., Chu, B. W., Sun, Y. L., and He, H.: Variations and sources of
652   nitrous acid (HONO) during a severe pollution episode in Beijing in winter 2016,
653   Sci Total Environ, 648, 253-262, 2019.
654   Zhang, Y. M., Wang, Y. Q., Zhang, X. Y., Shen, X. J., Sun, J. Y., Wu, L. Y., Zhang,
655   Z. X., and Che, H. C.: Chemical components, variation, and source Identification
656   of PM$_1$ during the heavy air pollution episodes in Beijing in December 2016, J
657   Meteorol Res-Prc, 32, 1-13, 2018.
658   Zhao, M. F., Xiu, G. L., Qiao, T., Li, Y. L., and Yu, J. Z.: Characteristics of haze
659   pollution episodes and analysis of a typical winter haze process in Shanghai,
660   Aerosol Air Qual Res, 16, 1625-1637, 2016.
661   Zhao, P. S., Dong, F., He, D., Zhao, X. J., Zhang, X. L., Zhang, W. Z., Yao, Q., and
662   Liu, H. Y.: Characteristics of concentrations and chemical compositions for
663   PM2.5 in the region of Beijing, Tianjin, and Hebei, China, Atmos Chem Phys,
664   13, 4631-4644, 2013.
665   Zheng, B., Tong, D., Li, M., Liu, F., Hong, C. P., Geng, G. N., Li, H. Y., Li, X., Peng,
666   L. Q., Qi, J., Yan, L., Zhang, Y. X., Zhao, H. Y., Zheng, Y. X., He, K. B., and
667   Zhang, Q.: Trends in China's anthropogenic emissions since 2010 as the
668   consequence of clean air actions, Atmos Chem Phys, 18, 14095-14111, 2018.
669

670   **Table 1**. The emission scenarios in WRF-Chem numerical experiments

Simulation scenarios	Descriptions
B0	Base simulation under the 2016 emission conditions.
N0	Same as B0, but only consider the gas-phase oxidation pathway for the production of nitrate aerosol.
C_N (N=1/2/…/8)	Same as B0, but anthropogenic NO_x emissions are reduced by 10%, 20%...80%, respectively, relative to the usual levels in 2016.
E1	Same as B0, but anthropogenic NO_x emissions are replaced using the MEIC inventory in 2012.

671

672   **Table 2**. Statistical evaluations of the model meteorological performance

Variable	Obs	Sim	R [a]	MB [a]	NMB [a]	ME [a]	RMSE [a]
Period I (15 August to 16 September)							
Temperature (℃)	24.04	23.91	0.89	−0.13	−0.55%	1.98	2.63
Humidity (%)	70.89	66.88	0.78	−4.01	−5.65%	11.07	14.67
Wind speed (m s^{-1})	2.46	3.04	0.50	0.58	23.72%	1.38	1.83
Period II (24 November to 26 December)							
Temperature (℃)	3.43	3.40	0.94	−0.03	−0.80%	2.18	2.83
Humidity (%)	69.85	65.27	0.63	−4.58	−6.56%	13.51	17.88
Wind speed (m s^{-1})	2.61	3.66	0.55	1.06	40.64%	1.70	2.23

673   [a] R: correlation efficient; MB: mean bias; NMB: normalized mean bias; ME: mean

674   error; RMSE: root mean square error.

675

676   **Table 3**. Statistical evaluations of the model chemical performance

Variable	Obs	Sim	MB	NMB	Obs	Sim	MB	NMB
	Period I				Period II			
$PM_{2.5}$	36.88	33.22	−3.66	−9.92%	91.59	64.28	−27.31	−29.82%
SO_2	17.65	16.51	−1.14	−6.46%	41.45	29.80	−11.65	−28.11%
NO_2	28.53	33.23	4.70	16.47%	53.01	54.28	1.27	2.40%
Daily-maximum O_3	237.45	255.77	18.32	7.72%	125.62	86.61	−39.01	−31.05%

677
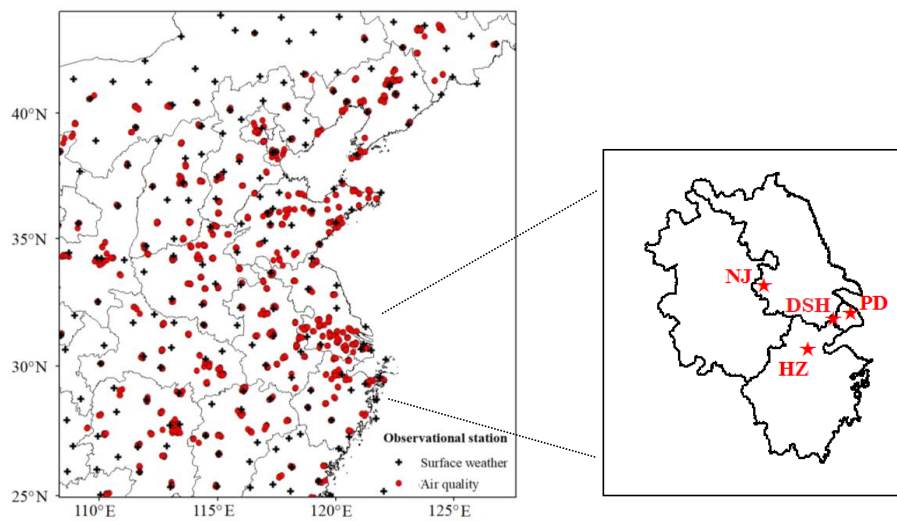
678   **Fig. 1**. WRF-Chem domain configuration and observational stations. Black crosses:

679   surface weather stations; Red dots: CNEMC routine air quality monitoring stations;

680   Red stars: surface supersites in YRD.

681

682

683
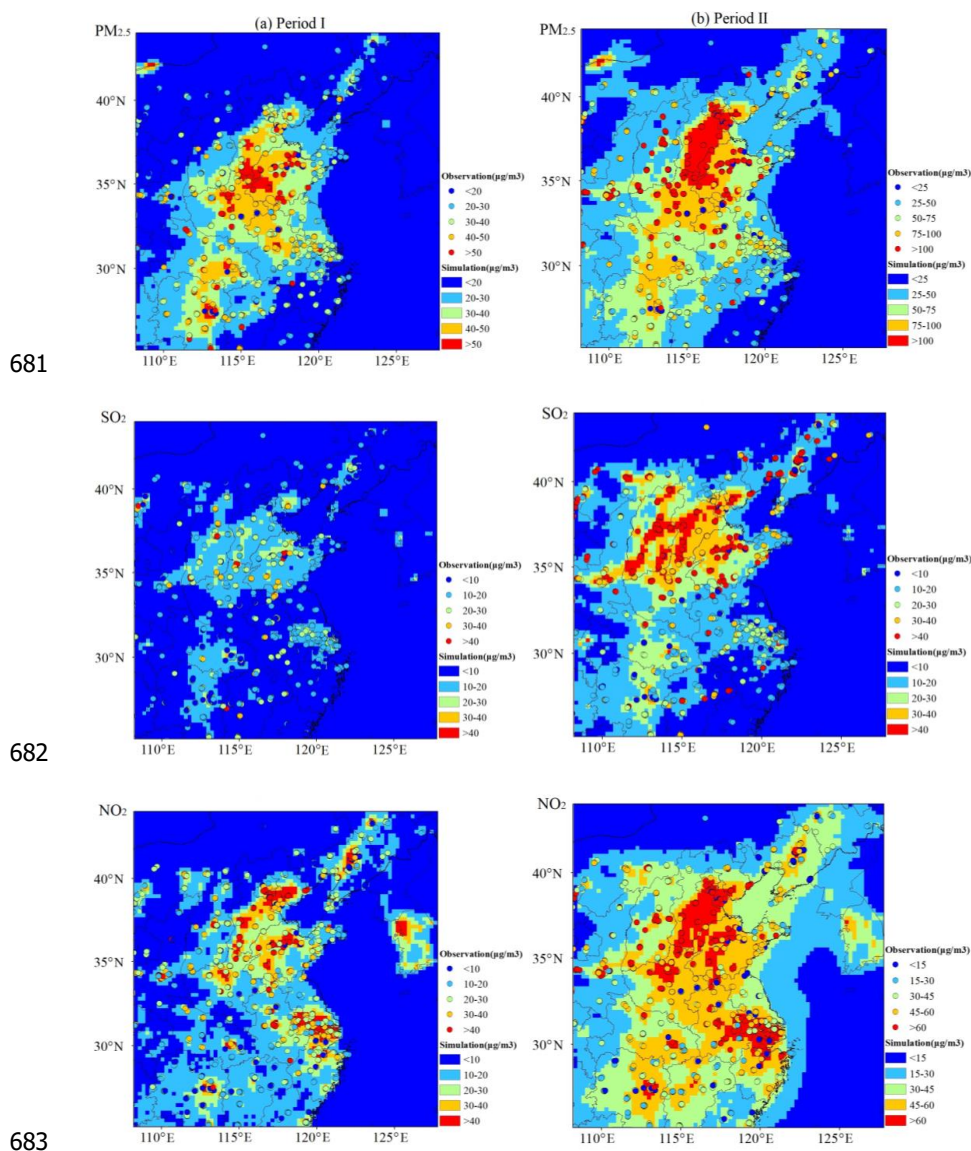
Fig. 2. Spatial patterns of the surface average PM$_{2.5}$, NO$_2$, SO$_2$ and daily-maximum O$_3$ concentrations in Period I (left panels) and Period II (right panels) from the WRF-Chem modeling (shaded contours) and routine air quality observations (dots).

684
685
686

687

688
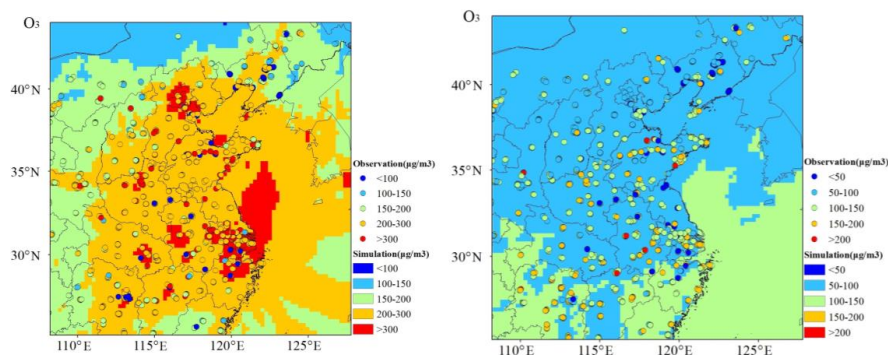
Fig. 2. Continued.

690
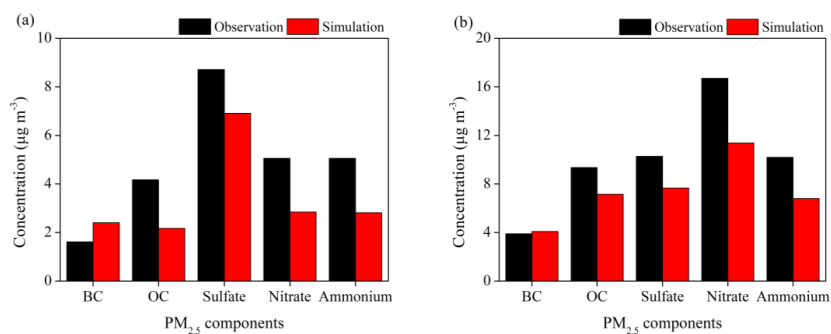
Fig. 3. Comparisons of surface PM$_{2.5}$ components from WRF-Chem simulations and observations in Period I (a) and Period II (b) at the four supersites in YRD.

693

694
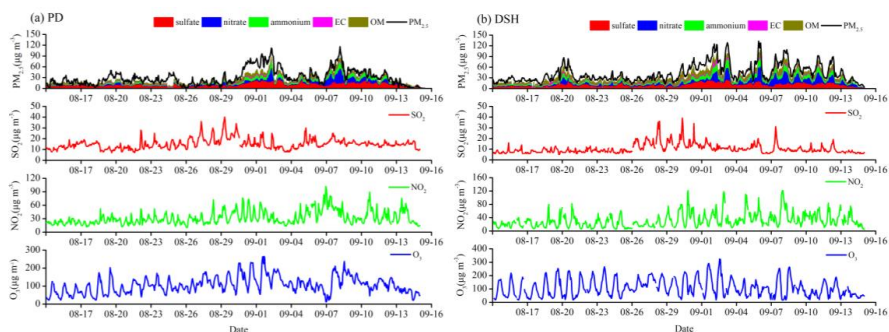
695
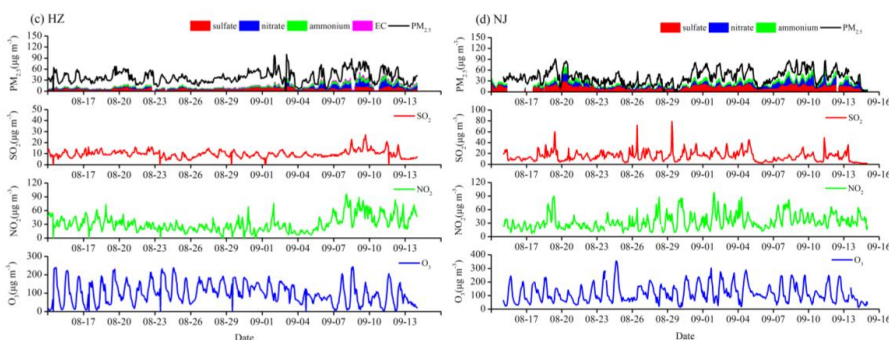
696   **Fig. 4**. Observed aerosol composition and gaseous pollutants concentrations at the

697   four supersites during Period I.

698

699
700
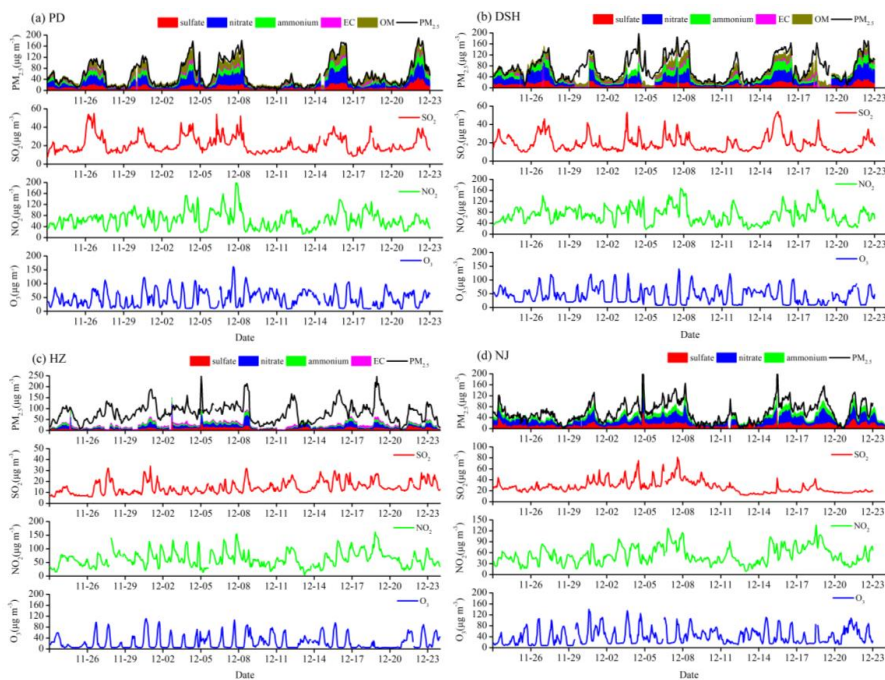
701 **Fig. 5**. Same as Fig. 3, but for Period II.

702
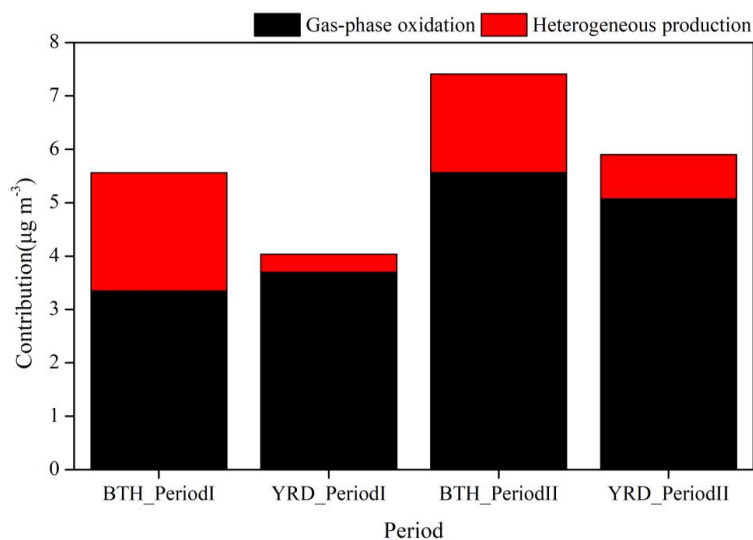
Fig. 6. Contributions of gas-phase oxidation and heterogeneous production to the surface nitrate concentrations for the BTH and YRD regions in two seasons.
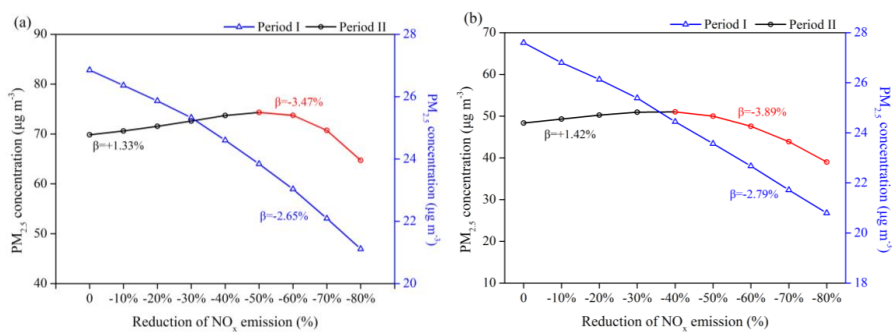
Fig. 7. Responses of surface PM$_{2.5}$ concentrations to the NO$_x$ emission reduction scenarios in (a) BTH and (b) YRD. The calculated NO$_x$ emission control efficiency (β) is also marked in the figure.

711
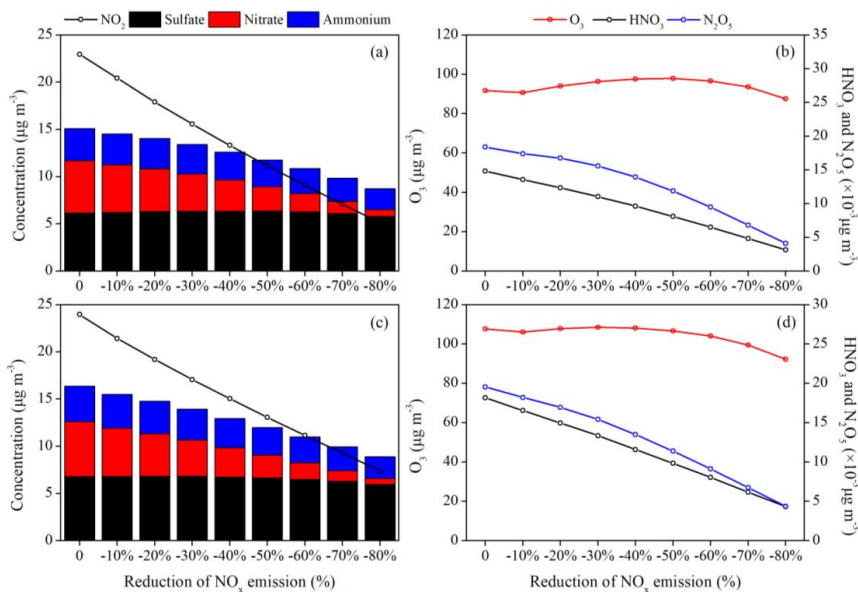
Fig. 8. Responses of the concentrations of surface SIA and key atmospheric trace gases (NO_2, O_3, HNO_3 and NO_3) to the NO_x emission reduction scenarios in (a, b) BTH and (c, d) YRD during Period I.
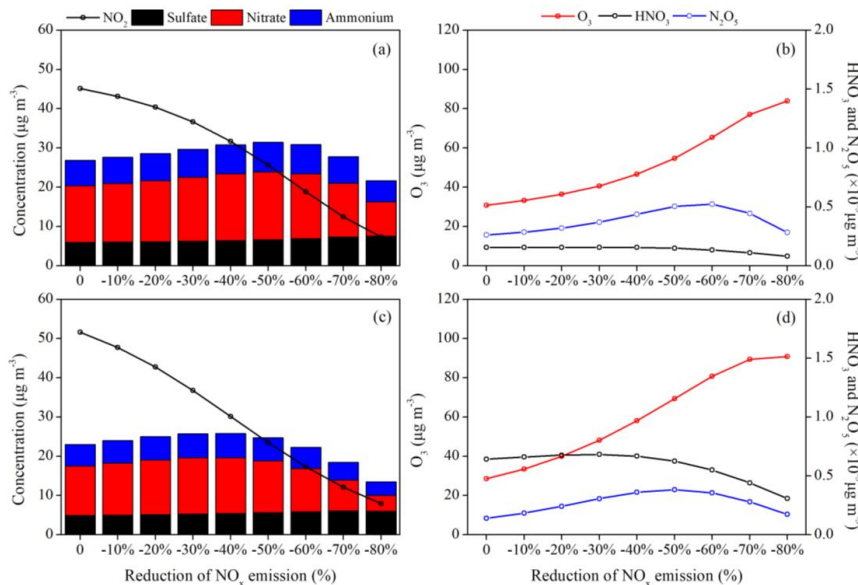
715

716   **Fig. 9**. Same as Fig. 7, but for Period II.

717
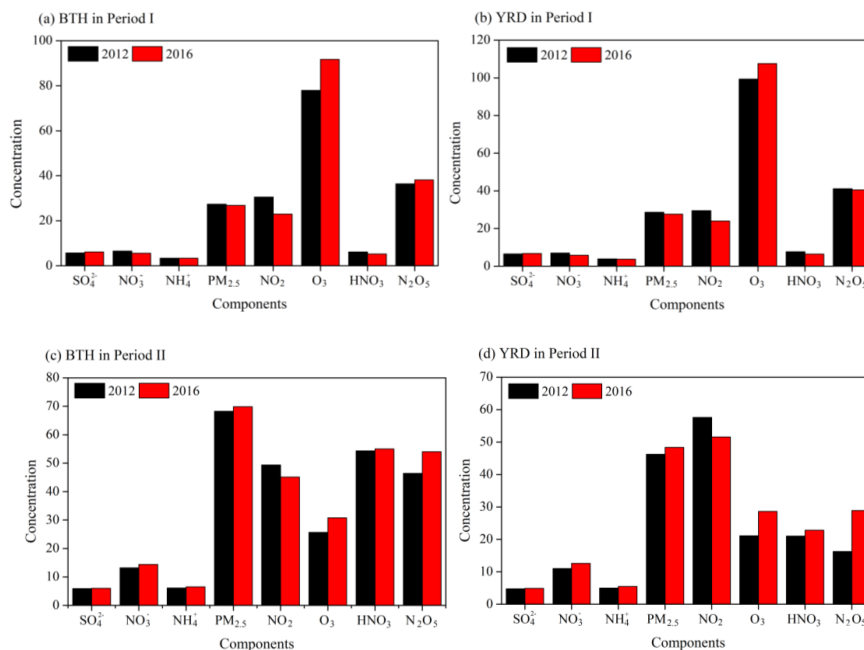
718

719

720 **Fig. 10**. Changes in the concentrations of surface $PM_{2.5}$, SIA components and key
721 atmospheric trace (NO_2, O_3, HNO_3 and N_2O_5) due to the 2012–2016 NO_x emission
722 reductions in China estimated as the differences between the base simulation and E1
723 scenario. The units are ppt for HNO_3 and N_2O_5, and $\mu g\ m^{-3}$ for other chemical species.